Running Title: WNT4 regulates cellular metabolism

Research article

WNT4 executes estrogen regulation of cellular metabolism via intracellular activity at the mitochondria

Joseph L. Sottnik[1+], Madeleine T. Shackleford[1+], Shaymaa Bahnassy[3], Zeynep Madak-Erdogan[4], Rebecca B. Riggins[3], Benjamin G. Bitler[2], Matthew J. Sikora[1]

[+]JLS and MTS contributed equally to this project.

Affiliations

[1]Dept. of Pathology, University of Colorado Anschutz Medical Campus

[2]Division of Reproductive Sciences, Dept. of Obstetrics and Gynecology, University of Colorado Anschutz Medical Campus

[3]Dept. of Oncology, Lombardi Comprehensive Cancer Center, Georgetown University

[4]Dept. of Food Science and Human Nutrition, Cancer Center at Illinois, Division of Nutritional Sciences, University of Illinois Urbana-Champaign

Corresponding author

Matthew J. Sikora, PhD.; Mail Stop 8104, Research Complex 1 South, Room 5117, 12801 E. 17th Ave.; Aurora, CO 80045. Tel: (303)724-4301; Fax: (303)724-3712; email: matthew.sikora@cuanschutz.edu. Twitter: @mjsikora

Authors' contributions

MJS conceived of the project. JLS and MTS designed and performed experiments. MTS developed models for the project. All authors contributed to data analysis and interpretation. MJS wrote the draft manuscript; all authors read and revised the manuscript and have read and approved of this version of the manuscript.

Key words

Invasive lobular carcinoma; WNT4; metabolism; breast cancer; estrogen; estrogen receptor

ABSTRACT

Invasive lobular carcinoma of the breast (ILC) has a distinct metabolic phenotype among breast cancer, characterized by relative metabolic quiescence and limited glucose uptake. However, recent work suggests ILC preferentially use fuels such as lipids and amino acids, and that ILC metabolism is linked to estrogen receptor α (ER) signaling. We previously reported that in ILC, estrogen-induced expression of Wnt ligand *WNT4* activates an atypical intracellular WNT4 pathway that regulates cellular metabolism and mitochondrial dynamics. However, mechanisms by which intracellular WNT4 regulates mitochondria are unknown. To address this, we performed proximity-dependent biotinylation with mass spectrometry (BioID) to profile WNT4 trafficking, localization, and intracellular functions. BioID showed that whereas canonical Wnt ligand WNT3A trafficked through the endoplasmic reticulum for secretion, WNT4 is predominantly in the cytosol and at the mitochondria. We also identified DHRS2, mTOR, and STAT1 as putative WNT4 cytosolic/mitochondrial signaling partners. These findings support a role for intracellular WNT4 regulating mitochondrial function and metabolism. We further investigated regulation of metabolism by ER-WNT4 using global metabolomics, following WNT4 knockdown versus over-expression compared to siRNA or small molecule inhibition of ER-WNT4 signaling. We found WNT4 signaling regulates oxidative phosphorylation (OXPHOS), with WNT4 knockdown suppressing OXPHOS as well as fatty acid and glutamate metabolism pathways, but not glycolytic activity. Taken together, WNT4 has atypical intracellular localization and signaling activity directly at the mitochondria that mediates ER regulation of cellular metabolism. ER-WNT4 signaling may play a key role in regulating the distinct metabolic phenotype of ILC by regulating mitochondrial activity and fuel usage.

INTRODUCTION

Invasive lobular carcinoma of the breast (ILC) is the most common special histological subtype of breast cancer, relative to breast cancer of no special type (i.e. invasive ductal carcinoma, IDC), accounting for up to 15% of breast cancer diagnoses [1–3]. ILC are presumed to be responsive to anti-estrogen therapies, since ~95% of ILC express estrogen receptor alpha (ER), but despite favorable biomarkers, ILC is associated with poor long-term outcomes and anti-estrogen resistance [1, 3–5]. The unique biology of ILC is understudied and poorly understood, hindering the development of ILC-targeted therapies and limiting advances in patient care.

ILC are considered metabolically quiescent compared to other ER+ breast cancers, based on cell line model studies and ILC tumor data. Du et al reported that both oxygen consumption rates (OCR, respiration) and extracellular acidification rates (ECAR, glycolysis) were reduced in ER+ ILC cell lines (MDA MB 134VI, SUM44PE, MDA MB 330) compared to ER+ IDC cell lines (MCF7, T47D, ZR751) [6]. In parallel, this study observed that genes differentially expressed in Luminal A ILC vs Luminal A IDC (n=1360) were strongly enriched for metabolic pathways, with overall reduced expression of genes involved in glucose metabolism in ILC vs IDC. Reduced glucose metabolism is also observed in clinical ILC tumor imaging - ILC tumors have on average ~40% reduced glucose uptake versus IDC in ^{18}F-fluorodeoxyglucose (FDG)/PET-CT imaging [7–12]. ILC tumors with no detectable FDG uptake are common, especially in metastatic ILC [8, 12, 13]. Similarly, tissue microarray studies showed ILC tumors express lower levels of glycolysis proteins (e.g. GLUT1/*SLC2A1*) by immunohistochemistry, but increased levels of oxidative phosphorylation proteins (e.g. GDH/*GLUD1*, SDHA) compared to IDC [14]. ILC tumors also show differential expression of lipid metabolism-related proteins [15], and accordingly, studies with anti-estrogen resistant ILC models identify increased lipid and glutamate metabolism as critical to the resistant phenotype [16–18]. Taken together, these observations suggest that ER+ ILC cells and tumors have a distinct metabolic phenotype compared to other breast cancers, including reduced glucose uptake and metabolism. However, the metabolic phenotype of ILC has not been mechanistically studied or defined.

ER signaling plays a central role in the regulation of cellular metabolism in ER+ breast cancer cells, including upregulation of gene expression in metabolic pathways, and activation of metabolic signaling cascades [19]. We reported that in ILC cells, ER induction of *WNT4* gene expression and WNT4 signaling controls mitochondrial dynamics and cell metabolism via an atypical mechanism of intracellular WNT4 signaling [20–22]. ER-WNT4 signaling was linked to mitochondrial protein MCL-1; WNT4 knockdown increased MCL-1 levels and drove mitochondrial fission or fragmentation [22]. Further, we found WNT4 knockdown impairs ATP production, manifesting as reduced ATP per cell and reduced respiratory capacity, ultimately resulting in cell death. These data support that ER-WNT4 signaling is critical in regulating ILC cell metabolism. However, the downstream mechanisms by which ER-WNT4, and intracellular WNT4 signaling, regulates metabolism and mitochondrial function in ILC cells are unknown but must be defined to understand the unique metabolic phenotype of ILC.

In this study, we used proximity biotinylation to profile WNT4 putative signaling partners and intracellular localization, and found intracellular WNT4 is localized to the mitochondria, where WNT4 mediates mitochondrial function and dynamics. We also used mass spectrometry-based metabolomics analyses to profile the metabolic effects of ER vs WNT4 signaling. These analyses corroborate a key role for WNT4 signaling downstream of ER in regulating cellular respiration, as well as in lipid and amino acid metabolism in ILC cells.

METHODS

Cell culture

MDA MB 134VI (MM134; RRID:CVCL_0617), HT1080 (RRID:CVCL_0317), and HT1080-A11 (*PORCN*-knockout, -PKO) were maintained as described [20, 21]. WNT4 over-expressing models (W4OE) and WNT3A over-expressing models were previously described and cultured in the same conditions as parental cell lines [21]. Wnt-BirA fusion expressing lines (described below) were also cultured as the parental cells. All lines were incubated at 37°C in 5% CO_2. Cell lines are authenticated annually via the University of Arizona Genetics Core cell line authentication service and confirmed mycoplasma negative every four months (most recently confirmed negative in June 2022). Authenticated cells were in continuous culture <6 months.

17β-Estradiol (E2; cat#2824), Z-4-hydroxytamoxifen (4OHT; cat#3412), and fulvestrant (fulv / ICI182,780; cat#1047) were obtained from Tocris Bioscience (Bio-Techne, Minneapolis, MN, USA) and dissolved in ethanol. Everolimus (evero; cat#11597) and PF-4708671 (PF; cat#15018) were obtained from Cayman Chemical (Ann Arbor, MI, USA) and dissolved in DMSO.

siRNAs were reverse transfected using RNAiMAX (ThermoFisher) according to the manufacturer's instructions. All constructs are siGENOME SMARTpool siRNAs (Dharmacon/Horizon Discovery, Lafayette, CO, USA), nontargeting pool #2 (D-001206-14-05), human *WNT4* (M-008659-03-0005), human *ESR1* (M-003401-04-0010).

Proximity-dependent biotinylation (BioID)

WNT3A and WNT4 were sub-cloned by Gateway recombination from the open-source Wnt library (Addgene Kit #1000000022) to the MAC-Tag-C vector (Addgene #108077) [23], generating Wnt ORFs with C-terminal BirA fusion (Wnt-BirA). Wnt-BirA plasmids were packaged for lentiviral transduction, and stably transduced into MM134, HT1080, and HT1080-PKO as previously described [21]. For proximity biotinylation analyses, parental and Wnt-BirA cells were treated with 50µM biotin (MilliporeSigma B4501) for 24 hours. Cells were then lysed with lysis buffer with 1% Triton X-100 (RPPA buffer [22]), and biotinylated proteins were extracted from the lysates using Pierce Streptavidin Magnetic Beads (ThermoFisher 88816) per the manufacturer's instructions.

Immunoblotting

Immunoblotting was performed as described [21, 22]. Blots were probed with Streptavidin-HRP (Cell Signaling #3999; RRID:AB_10830897) or antibodies used according to manufacturer's recommendations: WNT4 (R&D Systems, MAB4751; RRID:AB_2215448; also see specific immunoblotting considerations [21]); WNT3A (Novus Biologicals, MAB13242); anti-HA-HRP conjugate (Cell Signaling #2999; RRID:AB_1264166); DHRS2 (Sigma HPA053915; RRID:AB_2682307); mTOR (Cell Signaling #2983; RRID:AB_2105622); STAT1 (Sigma HPA000931; RRID:AB_1080100).

BioID - mass spectrometry analyses

For mass spectrometry analyses, cell lines (MM134, HT1080, HT1080-PKO; parental, WNT3A-BirA, and WNT4-BirA for each) were plated to 10cm plates in biological duplicate, and treated with 50µM biotin for 24 hours. Cells were lysed and extracted as above; sample/bead slurry was submitted for mass spectrometry analyses at the Central Analytical Mass Spectrometry Facility at the University of Colorado Boulder. Samples were eluted, reduced and alkylated with 2mM biotin in 5% (w/v) sodium dodecyl sulfate (SDS), 10 mM tris(2-carboxyethylphosphine) (TCEP), 40 mM 2-chloroacetamide, 50 mM Tris-HCl, pH 8.5 with boiling 10 minutes, then incubated shaking at 2000 rpm at 37°C for 30 minutes. Extracted proteins were digested using the SP3 method [24]. Briefly, 200 µg carboxylate-functionalized speedbeads (Cytiva Life Sciences) were added followed by the addition of acetonitrile to 80% (v/v) inducing binding to the beads. The beads were washed twice with 80% (v/v) ethanol and twice with 100% acetonitrile. Proteins were digested in 50 mM Tris-HCl, pH 8.5, with 0.5 µg Lys-C/Trypsin (Promega) and incubated at 37˚C overnight. Tryptic peptides were desalted using an rpC18 column with 0.1% (v/v) TFA in water and acetonitrile. Cleaned-up peptide were then dried in a speedvac vacuum centrifuge and stored at -20°C until analysis.

Tryptic peptides were suspended in 3% (v/v) ACN, 0.1% (v/v) trifluoroacetic acid (TFA) and directly injected onto a reversed-phase C18 1.7 µm, 130 Å, 75 mm X 250 mm M-class column (Waters), using an Ultimate 3000 nanoUPLC (Thermos Scientific). Peptides were eluted at 300 nL/minute with a gradient from 2% to 20% ACN in 100 minutes then to 32% ACN in 20 minutes followed by 1 minute to 95% ACN and detected using a Q-Exactive HF-X mass spectrometer (Thermo Scientific). Precursor mass spectra (MS1) were acquired at a resolution of 120,000 from 380 to 1580 m/z with an automatic gain control (AGC) target of 3E6 and a maximum injection time of 45 milliseconds. Precursor peptide ion isolation width for MS2 fragment scans was 1.4 m/z, and the top 12 most intense ions were sequenced. All MS2 spectra were acquired at a resolution of 15,000 with higher energy collision dissociation (HCD) at 27% normalized collision energy. An AGC target of 1E5 and 100 milliseconds maximum injection time was used. Dynamic exclusion was set for 25 seconds with a mass tolerance of ±10 ppm. Rawfiles were searched against the Human database (UP000005640) using MaxQuant v.1.6.14.0. Cysteine carbamidomethylation was considered a fixed modification, while methionine oxidation and protein N-terminal acetylation were searched as variable modifications. All peptide/protein identifications were at a threshold of 1% false discovery rate (FDR).

Label-free quantification (LFQ) data from MaxQuant were processed using LFQ-Analyst [25] to define differentially enriched proteins across Wnt-BioID studies. For comparisons, missing/zero values were imputed using Perseus-type or MinProb algorithms, with downstream hits required to be identified using both methods. Wnt-associated proteins were defined by increased LFQ vs control (parental cells without Wnt-BirA) with adjusted $p < 0.4$. Proteins identified in >20% of studies in the CRAPome database [26] were excluded from further analyses. Gene ontology analyses were performed using Enrichr [27], DAVID [28], and SubCell BarCode ([29], NetWork multi-protein localization tool).

Metabolomics analyses

MM134 cells were transfected with siRNA for 72 hours prior to harvest; MM134 and MM134-W4OE were treated with vehicle (0.6% DMSO), fulvestrant (100nM), 4OHT (100nM), everolimus (100nM), or PF-4708671 (30µM) for 48 hours prior to harvest. At harvest, cells were trypsinized and counted, then washed three times in PBS, and frozen as dry cell pellets prior to processing at the University of Colorado School of Medicine Metabolomics Core Facility. Metabolites were extracted from frozen cell pellets at 3 million cells per mL by vigorous vortexing in ice cold 5:3:2 MeOH:MeCN:water (v/v/v) for 30 min at 4C. Supernatants were clarified by centrifugation (10 min @ 12kxg, 4C). The resulting extracts were analyzed (10uL per injection) by ultra-high-pressure liquid chromatography coupled to mass spectrometry (UHPLC-MS — Vanquish and Q Exactive, Thermo). Metabolites were resolved on a Kinetex C18 column (2.1 x 150 mm, 1.7 um) using a 5-minute gradient method as previously described [30]. Following data acquisition, .raw files were converted to .mzXML using RawConverter then metabolites assigned and peaks integrated using Maven (Princeton University) in conjunction with the KEGG database and an in-house standard library. Quality control was assessed as using technical replicates run at beginning, end, and middle of each sequence as previously described [31]. Metabolite data was analyzed using Metaboanalyst 5.0 [32]; parameters for specific analyses described in text and in 'readme' sheets in associated supplemental data files.

Metabolic assays

XF96 (Agilent Technologies, 102417-100) extracellular flux assay kits were used to measure oxygen consumption (OCR) and glycolytic flux (ECAR) as described [33]. MM134 cells were reverse transfected with siRNA as above, and 24 hours later, cells were collected by trypsinization and re-plated to an XF96 microplate at 80k cells/well in 6 biological replicate wells per condition. 24 hours after re-plating (i.e. 48 hours after siRNA transfection), medium was replaced with Seahorse XF media (Agilent Technologies, 102353-100) an the plate was incubated at 37C for 30 min. After incubation, metabolic flux analyses were performed both at basal conditions and after injection of 5mg/ml oligomycin (Sigma-Aldrich, 871744), 2mM FCCP (Sigma-Aldrich, C2920), 5mM Antimycin A (Sigma-Aldrich, A8774), and 5mM rotenone (Sigma-Aldrich, R8875) (chemicals generously provided by the Jordan Laboratory, CU Anschutz). Outputs were normalized to total cell number.

Extracellular lactate was measured by Lactate-Glo assay (Promega, J5021). MM134 were reverse transfected with siRNA as above in 96-well plates (25k cells/well), and incubated for 6hr at 37C prior to time 0. At the indicated timepoints, 3µL of medium collected and diluted in PBS (1:250 dilution). At time course completion, samples were mixed 1:1 in assay sample buffer, and read per the manufacturer's instructions.

RESULTS

WNT4-BioID identifies distinct WNT4 intracellular localization to the mitochondria

Our prior work supports that intracellular WNT4 activity regulates mitochondrial function, but WNT4 localization and signaling partners for intracellular signaling are unknown. To profile WNT4 trafficking, localization, and novel intracellular functions, we performed proximity-dependent biotinylation (BioID) followed by mass spectrometry (MS). We expressed WNT4 or WNT3A fused to C-terminal BirA biotin ligase in HT1080 wild-type (WT) and HT1080-PORCN-null (PKO) cells (Wnt-responsive fibrosarcoma cell line), and ILC cell line MDA MB 134VI (MM134) (**Figure 1A-C**). We previously used these models to characterize WNT4 intracellular trafficking and signaling [21, 22]. Cells were treated with biotin for 24 hours, and then biotinylated proteins - i.e. those in proximity (within ~10 nm) to Wnt-BirA (**Figure 1C**) - were extracted and profiled by MS, with analysis as described in Methods. Raw data for BioID-MS is provided in **Supplemental File 1**.

We first needed to confirm that our BioID-MS approach could identify differential canonical WNT3A trafficking based on porcupine O-acetyltransferase (PORCN)-status (HT1080 vs HT1080-PKO; **Figure 1D**). In canonical Wnt trafficking, PORCN is required for Wnt interaction with Wntless (WLS) in the endoplasmic reticulum, subsequent WLS-mediated Wnt trafficking through the Golgi, and Wnt secretion, while PORCN ablation inhibits Wnt trafficking and secretion. Among n=184 WNT3A-associated proteins in HT1080, n=46 were enriched in HT1080 vs HT1080-PKO. These putative PORCN-dependent WNT3A-associated proteins (**Supplemental File 2**) included WLS (enriched >20-fold in HT1080 vs HT1080-PKO, **Figure 1E**), and were strongly enriched for Golgi localization (GO Cellular Compartment: trans-Golgi network, p=0.0024). These enrichments confirm that BioID identified the suppression of WNT3A trafficking to the Golgi in the PORCN-knockout context. Consistent with our previous observation of atypical (PORCN-independent) WNT4 trafficking and secretion [21], only n=8 WNT4-associated proteins were similarly enriched in HT1080 vs HT1080-PKO, suggesting PORCN-knockout had minimal impact on WNT4 trafficking.

We compared WNT4-associated (n=277) vs WNT3A-associated (n=184) proteins in HT1080 (**Figure 2A**). From the WNT4-specific proteins in HT1080 (n=172), we identified a subset of "high-confidence" WNT4-associated proteins based on increased signal intensity for WNT4-BioID vs control and WNT3A-BioID in at least 2 of 3 cell lines examined (n=72, **Figure 2A-B**, **Supplemental File 2**). From these subsets, we examined differential predicted localization using gene ontology and SubCell BarCode analysis (**Supplemental File 2**). Consistent with canonical Wnt secretion, WNT3A-associated proteins and WNT3A-specific proteins (n=79) were enriched for localization at the ER/Golgi (**Figure 2C**), and WNT3A was predicted to be located in the secretory pathway (**Figure 2D**). In contrast, WNT4-associated proteins and WNT4-specific proteins (n=172) were significantly enriched for mitochondrial proteins (adjusted $p=1.6x10^{-12}$, $=8.4x10^{-11}$, respectively, **Figure 2C¸Supplemental File 2**). Using SubCell barcode analysis [29], WNT4 was predicted to be located in the cytosol or at the mitochondria (**Figure 2D**). High-confidence WNT4-associated proteins were also enriched for mitochondrial proteins and predicted WNT4 localization at the mitochondria (**Figure 2B-D**). Notably, the high-confidence WNT4-associated proteins included both mitochondrial membrane and matrix proteins (**Figure 2E,** red text) as well as proteins involved in mitochondrial biogenesis/dynamics (**Figure 2E,** pink text), suggesting intra-mitochondrial WNT4 localization.

Among the most strongly enriched putative WNT4-associated proteins were mitochondrial reductase / dehydrogenase DHRS2, regulators of mitochondrial biogenesis, dynamics, and mitophagy (PIK3C3, PIK3R4, and mTOR), and STAT1, which can translocate to the mitochondria to regulate cellular metabolism [34–36]. We validated the proximity and putative association with WNT4 for DHRS2, mTOR, and STAT1 by streptavidin

pulldown and immunoblotting in independent samples (**Figure 2F**). These data support our BioID-MS findings and the putative role for WNT4 in regulating cellular metabolism and mitochondrial function.

Integrated transcriptome and metabolome data links ER to broad control of metabolism in ILC cells

We next examined how WNT4 controls metabolism in the context of the ER-WNT4 pathway in ILC, using untargeted mass spectrometry-based metabolomics to profile regulation of cellular metabolism by ER-WNT4 using ILC cell line MM134. The **Figure 3A** schematic summarizes the overall metabolomics study design. We targeted ER-WNT4 signaling directly using siRNA, and in parallel, compared inhibition of ER-WNT4 signaling in parental MM134 versus WNT4 over-expressing (W4OE) MM134 cells.

To first examine the role for ER in regulation of metabolism in ILC cells, we integrated metabolomics data with gene expression data in MM134 following ER knockdown [37], and performed joint pathway analysis of metabolites (n=63; **Figure 3B**) and genes (n=5322) dysregulated by *ESR1* siRNA (**Supplemental File 3**). Consistent with the central role for ER in cell proliferation, integrated pathway analysis showed enrichment in biosynthetic pathways, as well as glycolysis, the TCA cycle, and fatty acid metabolism (**Figure 3B**). Metabolite and gene expression changes after ER knockdown were consistent with decreased glycolysis and cellular respiration, and increased fatty acid metabolism (**Figure 3C**). Notably, while the levels of most TCA Cycle metabolites and associated genes decreased upon ER knockdown, expression of *IDH1* and level of onco-metabolite 2-hydroxyglutarate increased after ER knockdown (no *IDH1/2* mutations have been reported in MM134 cells). Overall, these data are consistent with previous reports on the critical role for ER in regulating cellular metabolism in ER+ breast cancer cells and confirm metabolic remodeling upon suppression of ER.

To examine how ER-mediated gene regulation may differentially regulate metabolism in ILC vs IDC cells, we identified genes regulated by treatment with 17β-estradiol in our transcriptomic data from ILC models MM134 and MM330 [37], IDC model HCC1428 [37], and consensus ER target genes across breast cancer cell lines ([38], primarily IDC model MCF7). Among shared estrogen-regulated genes, lipid metabolism pathways were strongly enriched (n=83 genes across enriched lipid metabolism-related genesets; **Supplemental File 4**). n=56 (67%) were similarly induced or repressed by estrogen in all 4 settings; only 2 genes were differentially regulated in ILC (MM134/MM330) vs IDC (HCC1428/consensus), *PPARD* and *SULT1A1*, and other differences were model-specific (**Supplemental Figure 1**). These data suggest that distinct downstream signaling pathways regulated by ER – for example, WNT4 signaling – rather than distinct transcriptional control of metabolic genes, are critical in differential regulation of metabolism by ER in ILC cells.

Metabolic effects of WNT4 knockdown support WNT4 as a key downstream mediator of ER signaling

WNT4 siRNA broadly dysregulated metabolite levels (n=77, **Figure 4A**), consistent with mitochondrial fission and decreased ATP levels upon WNT4 knockdown [22]. Metabolites dysregulated by WNT4 knockdown extensively overlapped the effects of ER knockdown (**Figure 4A-B**). Among the n=46 metabolites dysregulated by both WNT4 and ER knockdown (e.g. fatty acids, 2-hydroxyglutarate, glutamine), siWNT4 and siESR1 effects were strongly correlated ($\rho = 0.8435$, **Figure 4C**). supporting that WNT4 is a downstream mediator of ER-driven metabolic regulation in ILC cells. Pathway analysis confirmed that WNT4 and ER knockdown similarly impacted biosynthetic and metabolic pathways (**Figure 4D**), e.g. TCA cycle, fatty acid biosynthesis, and glutamate metabolism. WNT4 knockdown impacted the levels of more metabolites in pathways including unsaturated fatty acid biosynthesis (pathway enrichment: siESR1, p=0.79; siWNT4, p=0.033) and glutamine/glutamate metabolism (siESR1, p=0.26; siWNT4, p=0.017) (**Supplemental File 3**). While the metabolic impact of ER and WNT4 knockdown are tightly correlated, these differences suggest that a subset of the metabolic activities of WNT4 signaling are distinct from the global metabolic impacts of ER suppression.

WNT4 knockdown dysregulates cellular respiration but not glycolysis

We further examined the differential impact of ER vs WNT4 knockdown on cellular energetics using Seahorse metabolic flux analysis in MM134 cells (**Figure 5A**). Paralleling the observed effects on gene expression and metabolite levels in the TCA Cycle, *ESR1* or *WNT4* siRNA suppressed basal oxygen consumption rate (OCR; **Figure 5A-B**). However, after ER knockdown cells retained full spare respiratory capacity, whereas WNT4

knockdown caused a decrease in spare respiratory capacity (**Figure 5B**); this observation supports that WNT4 knockdown causes mitochondrial dysfunction [22]. Unlike the effects of WNT4 knockdown on respiration, we observed that siWNT4 had only a modest impact on extracellular acidification rate vs siESR1 (ECAR; **Figure 5C**). Accordingly, siESR1 reduced intracellular lactic acid levels in our metabolomics data while siWNT4 had no effect compared to control (**Figure 5D**), which we also observed by measuring lactic acid secretion (**Figure 5E**). The differential effect on ECAR and lactic acid levels demonstrate distinct WNT4-mediated metabolic regulation independent of glycolytic activity.

Since WNT4 knockdown suppresses ILC cell ATP levels and dysregulates oxygen consumption/respiration, but not glycolysis, we hypothesized that ILC cells are relatively more reliant on OXPHOS versus glycolysis for energy production. In cellular dependency screens (public Depmap data [39]), ILC cell lines are uniquely sensitive to suppression of genes involved in pyruvate metabolism. We examined 15 genes in glucose metabolism and pyruvate synthesis in ER+ cell lines (n=25). ILC cell lines (n=3; MM134, 44PE, MM330) were in the top 4 lines most sensitive to knockdown of genes in this pathway (**Figure 5F**) and clustered independently from other ER+ lines (**Figure 5G**, left). ILC-like cell line CAMA1 [37, 40] was similarly overall sensitive to knockdown of pyruvate production genes (**Figure 5F**). This phenotype was specific for pyruvate production as TCA cycle genes (e.g. *OGDH*) were broadly essential across ER+ breast cancer cell lines (**Figure 5G**, right). Taken together, WNT4 signaling is necessary for ILC cellular respiration; glycolysis is maintained with WNT4 knockdown but is insufficient to maintain ILC cell viability, as ILC cells are more dependent on cellular respiration via pyruvate production.

WNT4 signaling is integrated in an ER-mTOR pathway and is critical for lipid metabolism

Our metabolomics study also compared the effects of small molecule inhibitors of the ER-WNT4 signaling pathway on parental MM134 vs WNT4-overexpressing (W4OE) MM134 (**Figure 6A**). We hypothesized that WNT4 over-expression would rescue a subset of inhibitor-mediated metabolic effects and indicate direct WNT4 signaling effects. Two-factor analysis (W4OE vs. Parental, controlled for drug effect) identified that WNT4-overexpression significantly altered the levels of 71 metabolites (**Figure 6B**), of which 38 overlapped with siWNT4. The effects of W4OE vs. siWNT4 were inverse for the majority of these metabolites (n=22; **Figure 6C**), supporting direct WNT4 regulation of metabolites including glucose, glutamate, 2-hydroxyglutarate, and fatty acids (n=7) (**Supplemental File 5**).

We further examined whether WNT4 over-expression rescued the metabolic effects of individual inhibitors. The effects of mTOR inhibitor everolimus and S6 Kinase inhibitor PF-4708671 on parental vs W4OE cells were strongly correlated (**Figure 6D**), suggesting that WNT4-overexpression has a limited capacity to override inhibition of downstream signaling. Similarly, the effects of anti-estrogen fulvestrant were highly correlated in parental vs W4OE, as WNT4 may be insufficient to overcome complete ER inhibition in ER-dependent breast cancer cells. However, a larger subset of effects of 4OH-tamoxifen were reversed in W4OE cells, consistent with tamoxifen partial agonist activity in these cells [20] – incomplete inhibition of ER by 4OH-tamoxifen (i.e. tamoxifen resistance) can be partially rescued by WNT4-overexpression. From these data, we identified n=38 metabolites for which effects of ≥2 inhibitors were reversed by ≥30% (**Figure 6E**), which were enriched for fatty esters (i.e. carnitines, n=4, p=0.032), supporting a key role for WNT4 in fatty acid/lipid metabolism.

Integrating WNT4-regulated metabolic pathways in siRNA, over-expression, and inhibitor studies identified n=41 metabolites differentially regulated by activation vs suppression of WNT4 signaling (**Figure 7A**, **Supplemental File 6**). Enrichment analysis of these consensus WNT4-regulated metabolites identified the arginine and proline metabolic pathway, which supports a role for WNT4 signaling in glutamate metabolism. Further, fatty acid biosynthesis and metabolism were key pathways/metabolites regulated via WNT4 signaling (**Figure 7B**).

Our data on ER-WNT4 signaling highlights a putative role for lipid metabolism in the distinct metabolic phenotype of ILC. To examine this in tumor data, we performed gene set enrichment analyses from n=1360 genes differentially expressed in ER+ Luminal A ILC versus IDC [6]. Using Wikipathways, 4 of the top 8 over-represented pathways were metabolic, with an increase in genes associated with lipid metabolism in ILC vs

IDC (**Figure 7C**, **Supplemental File 7**). Metabolic pathways were also enriched in Hallmark gene signatures, with an increase in genes associated with Adipogenesis and Fatty acid metabolism, versus a decrease in genes associated with Glycolysis and Oxidative Phosphorylation, in ILC vs IDC (**Figure 7C**). Using functional gene set enrichment analyses, differential gene expression in ILC is consistent with decreased glycolysis/OXPHOS and increased fatty acid metabolism (**Figure 7D**, **Supplemental File 7**). These data support that ER-WNT4 signaling at least in part drives increased lipid metabolism as part of the distinct metabolic phenotype of ILC.

DISCUSSION

Data from laboratory models, tumor studies, and clinical imaging studies support that ILC has a distinct metabolic phenotype relative to other ER+ breast cancers, and we hypothesized that an ER-WNT4 signaling pathway plays a key role in the regulation of ILC cell metabolism and mitochondrial function. We investigated the potential mechanisms by which WNT4 regulates metabolism and mitochondrial function using BioID, which support our prior work showing that while WNT3A is trafficked via canonical secretory pathways, WNT4 is instead localized to the cytosol and mitochondria. Using untargeted metabolomics analyses, we found that WNT4 is a key downstream effector of ER-driven metabolic remodeling in ILC cells, and that WNT4 signaling regulates cellular respiration, amino acid metabolism, and fatty acid metabolism. Taken together, ER-mediated activation of intracellular WNT4 signaling is a key component of estrogen regulation of ILC cell metabolism and the distinct metabolic phenotype of ILC tumors.

The limited avidity for FDG in PET-CT imaging strongly suggests that ILC tumors preferentially utilize fuels other than glucose, such as amino acids and/or fatty acids, in particular in the context of advanced anti-estrogen-resistant ILC. Studies from the Riggins Laboratory have shown that ILC cell lines are uniquely sensitive to inhibition of glutamate transport using riluzole, especially in combination with ER inhibition [17, 18]. Similarly, in a panel of breast tumor explant cultures (n=5) including one ILC, the ILC was unique in being growth suppressed by single agent riluzole and combined riluzole + fulvestrant [18]. Studies from the Oesterreich Lab identified upregulation of *SREBP* and *FASN* to be critical to anti-estrogen resistance in ILC; endocrine resistant ILC cell line variants were hypersensitive to SREBP knockdown or inhibition versus the parental cells, or CPT1 inhibitor etomoxir [16]. In tissue microarray analyses (ILC n=108, IDC n=584), nearly all ILC were positive for hormone-sensitive lipase (HSL/*LIPE*), which hydrolyzes triglycerides into free fatty acids, while this was uncommon in IDC (HSL+: 93% ILC v 15% IDC) [15]. Similarly, fatty acid transporter FABP4 was expressed in 32% of ILC vs <2% of IDC, supporting that ILC may require greater fatty acid utilization than IDC. While our analyses of ER-WNT4 signaling support that this pathway underpins fatty acid metabolism in ILC cells, limited data exist on the mechanisms underlying differential metabolic activity, including fatty acid metabolism, in ILC. Notably, recent work from the Madak-Erdogan Laboratory shows that the tumor microenvironment and metastatic niche can dramatically reprogram ER-driven cellular metabolism [41]. Given that ILC metastasize to distinct sites versus IDC (e.g. peritoneum, gastrointestinal tract, ovary) [3, 42, 43], and also uniquely interact with and remodel the tumor microenvironment [44, 45], ER-WNT4 signaling may integrate microenvironmental signals to regulate metabolism in ILC.

Metabolite tracing studies in ILC cells have not previously been reported, and as such, the flux of glucose and other metabolites has not been profiled. Future studies using radio-labeled tracers are critical to understand differential glucose vs glutamine/glutamate utilization, and whether ER-WNT4 regulation of fatty acid metabolism impacts uptake vs biosynthesis. Similarly, though ILC are less FDG-avid, the impact of therapy and disease progression on ILC metabolism (and thus FDG avidity) has not been extensively explored outside of anti-estrogen resistant cell line variants. Stires et al reported that while single agent riluzole did not impact growth of ILC PDX HCI-013EI (an estrogen-independent outgrowth of parental HCI-013), combining riluzole with fulvestrant delayed tumor growth longer than fulvestrant alone, supporting that glutamate metabolism is important in ILC tumor response to fulvestrant *in vivo* [18]. Further, ILC PDX HCI-013 showed intra-tumor

metabolic heterogeneity, which was greater in the endocrine resistant HCI-013EI [46]. Tumor metabolite tracing, PET-CT studies pairing FDG with other tracers (e.g. ^{18}F-fluoroestradiol [8, 12]), and alternative imaging approaches [47], may facilitate further study of ILC tumor metabolism and metabolic remodeling during therapy response and resistance, and disease progression.

WNT4 localization to the mitochondria as predicted by BioID links our prior discovery of atypical intracellular localization and function of WNT4 [21], with our findings on WNT4 regulation of mTOR signaling, ATP production, and mitochondrial dynamics [22]. In the latter study, we found that WNT4 is integral in downstream mTOR signaling via S6 Kinase; WNT4 was necessary for S6 Kinase and S6 phosphorylation, but not mTOR phosphorylation. In the current study, we identified mTOR as a putative WNT4-associated protein. Though our data do not necessarily distinguish proximity vs direct interaction, taken together, WNT4 may serve to regulate mTOR interaction with or access to downstream partners like S6 Kinase. Mechanistic links between WNT4 and DHRS2 or STAT1 have not been reported. While the function of DHRS2 (aka Hep27) is not well characterized, DHRS2 is primarily mitochondrial (in addition to nuclear forms) and has been linked to oxidative stress and remodeling of lipid metabolism [48, 49]. While STAT1 is primarily considered cytosolic en route to the nucleus, STAT1 regulates mitochondrial dynamics/biogenesis [35] and has been reported to localize to the mitochondria and regulate respiration [34, 36]. Future studies will further examine the discrete localization of WNT4 at/within the mitochondria, mechanisms of trafficking, and direct protein interactions. Defining tissue-specific WNT4 activity as a canonical, non-canonical, or intracellular Wnt ligand are also an important future direction, and we recently reviewed the distinct roles for WNT4 in reproductive and gynecologic tissues versus other tissues [50].

ILC has a unique metabolic phenotype among breast cancers, clinically indicated by reduced glucose uptake, and mechanistically indicated by relative quiescence but increased amino acid metabolism and fatty acid metabolism. We show that ER signaling underpins cellular metabolism in ILC cells, in large part via regulation of WNT4 signaling. WNT4 regulates a subset of ER-driven metabolism, as WNT4 knockdown has only a minor effect of glycolysis, but dysregulates oxidative phosphorylation, glutamate metabolism, and fatty acid metabolism. These effects of ER-WNT4 signaling may be through novel, atypical effects of intracellular WNT4 directly at the mitochondria. Delineating differential ILC metabolism and the role of ER-WNT4 can define unique metabolic dependencies in ILC, shedding light on ILC etiology and identifying new treatment strategies.

ACKNOWLEDGEMENTS

The authors wish to thank Dr. Julie Haines and the University of Colorado School of Medicine Metabolomics Core, and Dr. Chris Ebmeier and the Central Analytical Mass Spectrometry Facility at the University of Colorado Boulder, for their contributions to this project. We thank Dr. Courtney Jones and the Craig Jordan Laboratory for technical assistance with Seahorse metabolic flux analyses.

FUNDING

This work was supported by R00 CA193734 (MJS) from the National Institutes of Health, by a grant from the Cancer League of Colorado, Inc (MJS), and by support from the Tumor-Host Interactions Program at the University of Colorado Cancer Center (MJS). This work was supported by the Office of the Assistant Secretary of Defense for Health Affairs through the Breast Cancer Research Program under Award No. W81XWH-17-1-0615 (RBR). This study utilized University of Colorado Cancer Center shared resources, which are supported in part by the National Cancer Institute through Cancer Center Support Grant P30CA046934. This study utilized the Central Analytical Mass Spectrometry Facility at the University of Colorado Boulder, supported in part by the National Institutes of Health support grant S10OD025267. Opinions, interpretations, conclusions,

and recommendations are those of the authors and are not necessarily endorsed by the Department of Defense or the National Institutes of Health.

REFERENCES

1. Sikora MJ, Jankowitz RC, Dabbs DJ, Oesterreich S. Invasive lobular carcinoma of the breast: patient response to systemic endocrine therapy and hormone response in model systems. Steroids. Elsevier Inc.; 2013 Jun;78(6):568–575. PMID: 23178159
2. Ciriello G, Gatza ML, Beck AH, Wilkerson MD, Rhie SK, Pastore A, et al. Comprehensive Molecular Portraits of Invasive Lobular Breast Cancer. Cell. 2015 Oct 8;163(2):506–19. PMID: 26451490
3. Mouabbi JA, Hassan A, Lim B, Hortobagyi GN, Tripathy D, Layman RM. Invasive lobular carcinoma□: an understudied emergent subtype of breast cancer. Breast Cancer Res Treat. Springer US; 2022;(0123456789):8–12.
4. Thomas M, Kelly ED, Abraham J, Kruse M. Invasive lobular breast cancer: A review of pathogenesis, diagnosis, management, and future directions of early stage disease. Semin Oncol. Elsevier Inc.; 2019;46(2):121–132. PMID: 31239068
5. Metzger Filho O, Giobbie-Hurder A, Mallon E, Gusterson B, Viale G, Winer EP, et al. Relative Effectiveness of Letrozole Compared With Tamoxifen for Patients With Lobular Carcinoma in the BIG 1-98 Trial. J Clin Oncol. 2015 Sep 1;33(25):2772–9. PMID: 26215945
6. Du T, Zhu L, Levine KM, Tasdemir N, Lee A V., Vignali DAA, et al. Invasive lobular and ductal breast carcinoma differ in immune response, protein translation efficiency and metabolism. Sci Rep. Springer US; 2018;8(1):7205. PMID: 29739984
7. Fujii T, Yajima R, Kurozumi S, Higuchi T, Obayashi S, Tokiniwa H, et al. Clinical Significance of 18F-FDG-PET in Invasive Lobular Carcinoma. Anticancer Res. 2016;36(10):5481–5485. PMID: 27798919
8. Ulaner GA, Jhaveri K, Chandarlapaty S, Hatzoglou V, Riedl CC, Lewis JS, et al. Head-to-Head Evaluation of 18F-FES and 18F-FDG PET/CT in Metastatic Invasive Lobular Breast Cancer. J Nucl Med. 2021;62(3):326–331. PMID: 32680923
9. Hogan MP, Goldman DA, Dashevsky B, Riedl CC, Gönen M, Osborne JR, et al. Comparison of 18F-FDG PET/CT for Systemic Staging of Newly Diagnosed Invasive Lobular Carcinoma Versus Invasive Ductal Carcinoma. J Nucl Med. 2015 Nov;56(11):1674–80. PMID: 26294295
10. Ulaner GA, Goldman DA, Gönen M, Pham H, Castillo R, Lyashchenko SK, et al. Initial Results of a Prospective Clinical Trial of 18F-Fluciclovine PET/CT in Newly Diagnosed Invasive Ductal and Invasive Lobular Breast Cancers. J Nucl Med. 2016 Sep;57(9):1350–6. PMID: 26940766
11. Ueda S, Tsuda H, Asakawa H, Shigekawa T, Fukatsu K, Kondo N, et al. Clinicopathological and prognostic relevance of uptake level using 18F-fluorodeoxyglucose positron emission tomography/computed tomography fusion imaging (18F-FDG PET/CT) in primary breast cancer. Jpn J Clin Oncol. 2008 Apr;38(4):250–8. PMID: 18407934
12. Venema C, de Vries E, Glaudemans A, Poppema B, Hospers G, Schröder C. 18F-FES PET Has Added Value in Staging and Therapy Decision Making in Patients With Disseminated Lobular Breast Cancer. Clin Nucl Med. 2017 Jun;42(8):1. PMID: 28604479
13. Ravina M, Saboury B, Chauhan MS, Jacob MJ, Pandit AG, Sanchety N, et al. Utility of 18 F-FDG PET/CT in pre-surgical risk stratification of patients with breast cancer. Hell J Nucl Med. 22(3):165–171. PMID: 31587025
14. Kim YH, Jung WH, Koo JS. Expression of metabolism-related proteins in invasive lobular carcinoma: comparison to invasive ductal carcinoma. Tumour Biol. 2014 Oct;35(10):10381–93. PMID: 25053597
15. Cha YJ, Kim HM, Koo JS. Expression of Lipid Metabolism-Related Proteins Differs between Invasive Lobular Carcinoma and Invasive Ductal Carcinoma. Int J Mol Sci. 2017 Jan 23;18(1):232. PMID: 28124996
16. Du T, Sikora MJ, Levine KM, Tasdemir N, Riggins RB, Wendell SG, et al. Key regulators of lipid metabolism drive endocrine resistance in invasive lobular breast cancer. Breast Cancer Res. 2018 Sep 4;20(1):106. PMID: 30180878
17. Stires H, Heckler MM, Fu X, Li Z, Grasso CS, Quist MJ, et al. Integrated molecular analysis of Tamoxifen-resistant invasive lobular breast cancer cells identifies MAPK and GRM/mGluR signaling as therapeutic vulnerabilities. Mol Cell Endocrinol. 2018;471:105–117. PMID: 28935545
18. Stires H, Olukoya AO, Ma S, Persaud S, Guerra Y, Cruz MI, et al. Riluzole suppresses growth and enhances response to endocrine therapy in ER+ breast cancer. bioRxiv. 2020 Jan

1;2020.07.30.227561.
19. Kulkoyluoglu-Cotul E, Arca A, Madak-Erdogan Z. Crosstalk between Estrogen Signaling and Breast Cancer Metabolism. Trends Endocrinol Metab. 2019;30(1):25–38. PMID: 30471920
20. Sikora MJ, Cooper KL, Bahreini A, Luthra S, Wang G, Chandran UR, et al. Invasive lobular carcinoma cell lines are characterized by unique estrogen-mediated gene expression patterns and altered tamoxifen response. Cancer Res. 2014 Mar 1;74(5):1463–74. PMID: 24425047
21. Rao DM, Shackleford MT, Bordeaux EK, Sottnik JL, Ferguson RL, Yamamoto TM, et al. Wnt family member 4 (WNT4) and WNT3A activate cell-autonomous Wnt signaling independent of porcupine O-acyltransferase or Wnt secretion. J Biol Chem. 2019 Dec 27;294(52):19950–19966. PMID: 31740580
22. Shackleford MT, Rao DM, Bordeaux EK, Hicks HM, Towers CG, Sottnik JL, et al. Estrogen Regulation of mTOR Signaling and Mitochondrial Function in Invasive Lobular Carcinoma Cell Lines Requires WNT4. Cancers (Basel). 2020 Oct 12;12(10). PMID: 33053661
23. Liu X, Salokas K, Tamene F, Jiu Y, Weldatsadik RG, Öhman T, et al. An AP-MS- and BioID-compatible MAC-tag enables comprehensive mapping of protein interactions and subcellular localizations. Nat Commun. 2018 Mar 22;9(1):1188. PMID: 29568061
24. Hughes CS, Foehr S, Garfield DA, Furlong EE, Steinmetz LM, Krijgsveld J. Ultrasensitive proteome analysis using paramagnetic bead technology. Mol Syst Biol. 2014 Oct 30;10:757. PMID: 25358341
25. Shah AD, Goode RJA, Huang C, Powell DR, Schittenhelm RB. LFQ-Analyst: An Easy-To-Use Interactive Web Platform To Analyze and Visualize Label-Free Proteomics Data Preprocessed with MaxQuant. J Proteome Res. 2020;19(1):204–211. PMID: 31657565
26. Mellacheruvu D, Wright Z, Couzens AL, Lambert J-P, St-Denis NA, Li T, et al. The CRAPome: a contaminant repository for affinity purification-mass spectrometry data. Nat Methods. 2013 Aug;10(8):730–6. PMID: 23921808
27. Xie Z, Bailey A, Kuleshov M V, Clarke DJB, Evangelista JE, Jenkins SL, et al. Gene Set Knowledge Discovery with Enrichr. Curr Protoc. 2021 Mar;1(3):e90. PMID: 33780170
28. Sherman BT, Hao M, Qiu J, Jiao X, Baseler MW, Lane HC, et al. DAVID: a web server for functional enrichment analysis and functional annotation of gene lists (2021 update). Nucleic Acids Res. 2022 Mar 23; PMID: 35325185
29. Orre LM, Vesterlund M, Pan Y, Arslan T, Zhu Y, Fernandez Woodbridge A, et al. SubCellBarCode: Proteome-wide Mapping of Protein Localization and Relocalization. Mol Cell. 2019;73(1):166-182.e7. PMID: 30609389
30. Nemkov T, Reisz JA, Gehrke S, Hansen KC, D'Alessandro A. High-Throughput Metabolomics: Isocratic and Gradient Mass Spectrometry-Based Methods. Methods Mol Biol. 2019;1978:13–26. PMID: 31119654
31. Nemkov T, Hansen KC, D'Alessandro A. A three-minute method for high-throughput quantitative metabolomics and quantitative tracing experiments of central carbon and nitrogen pathways. Rapid Commun Mass Spectrom. 2017 Apr 30;31(8):663–673. PMID: 28195377
32. Pang Z, Zhou G, Ewald J, Chang L, Hacariz O, Basu N, et al. Using MetaboAnalyst 5.0 for LC-HRMS spectra processing, multi-omics integration and covariate adjustment of global metabolomics data. Nat Protoc. 2022 Jun 17; PMID: 35715522
33. Jones CL, Stevens BM, D'Alessandro A, Reisz JA, Culp-Hill R, Nemkov T, et al. Inhibition of Amino Acid Metabolism Selectively Targets Human Leukemia Stem Cells. Cancer Cell. Elsevier Inc.; 2018;34(5):724-740.e4. PMID: 30423294
34. Meier JA, Larner AC. Toward a new STATe: the role of STATs in mitochondrial function. Semin Immunol. 2014 Feb;26(1):20–8. PMID: 24434063
35. Sisler JD, Morgan M, Raje V, Grande RC, Derecka M, Meier J, et al. The Signal Transducer and Activator of Transcription 1 (STAT1) Inhibits Mitochondrial Biogenesis in Liver and Fatty Acid Oxidation in Adipocytes. PLoS One. 2015;10(12):e0144444. PMID: 26689548
36. Bourke LT, Knight RA, Latchman DS, Stephanou A, McCormick J. Signal transducer and activator of transcription-1 localizes to the mitochondria and modulates mitophagy. JAK-STAT. 2013 Oct 1;2(4):e25666. PMID: 24470977
37. Sottnik JL, Bordeaux EK, Mehrotra S, Ferrara SE, Goodspeed AE, Costello JC, et al. Mediator of DNA damage checkpoint 1 (MDC1) is a novel estrogen receptor co-regulator in invasive lobular carcinoma of

the breast. Mol Cancer Res. 2021 May 4;1:1–14. PMID: 33947745

38. Ochsner SA, Abraham D, Martin K, Ding W, McOwiti A, Kankanamge W, et al. The Signaling Pathways Project, an integrated 'omics knowledgebase for mammalian cellular signaling pathways. Sci data. 2019;6(1):252. PMID: 31672983
39. Tsherniak A, Vazquez F, Montgomery PG, Weir BA, Kryukov G, Cowley GS, et al. Defining a Cancer Dependency Map. Cell. 2017 Jul 27;170(3):564-576.e16. PMID: 28753430
40. Michaut M, Chin S-F, Majewski I, Severson TM, Bismeijer T, de Koning L, et al. Integration of genomic, transcriptomic and proteomic data identifies two biologically distinct subtypes of invasive lobular breast cancer. Sci Rep. 2016 Jan 5;6:18517. PMID: 26729235
41. Zuo Q, Mogol AN, Liu Y-J, Santaliz Casiano A, Chien C, Drnevich J, et al. Targeting metabolic adaptations in the breast cancer-liver metastatic niche using dietary approaches to improve endocrine therapy efficacy. Mol Cancer Res. 2022 Feb 23;1–15. PMID: 35259269
42. Arpino G, Bardou VJ, Clark GM, Elledge RM. Infiltrating lobular carcinoma of the breast: tumor characteristics and clinical outcome. Breast Cancer Res. 2004 Jan;6(3):R149-56. PMID: 15084238
43. Mathew A, Rajagopal PS, Villgran V, Sandhu GS, Jankowitz RC, Jacob M, et al. Distinct Pattern of Metastases in Patients with Invasive Lobular Carcinoma of the Breast. Geburtshilfe Frauenheilkd. 2017 Jun;77(6):660–666. PMID: 28757653
44. Sflomos G, Battista L, Aouad P, De Martino F, Scabia V, Stravodimou A, et al. Intraductal xenografts show lobular carcinoma cells rely on their own extracellular matrix and LOXL1. EMBO Mol Med. 2021 Feb 5;13(3):e13180. PMID: 33616307
45. Gómez-Cuadrado L, Bullock E, Mabruk Z, Zhao H, Souleimanova M, Noer PR, et al. Characterisation of the Stromal Microenvironment in Lobular Breast Cancer. Cancers (Basel). 2022 Feb 11;14(4). PMID: 35205651
46. Olukoya A, Bahnassy S, Spoelstra NS, Jin L, Ranjit S, Elias A, et al. Abstract 1639: Human immune system mouse model of ER+ metastatic breast cancer. Cancer Res. 2022 Jun 15;82(12_Supplement):1639.
47. Torrado B, Vallmitjana A, Olukoya A, Bahnassy S, Stires H, Rozeboom A, et al. Abstract 2461: Integrated lifetime and spectral phasor imaging of biomarker expression and metabolism in hormone receptor positive breast cancer models. Cancer Res. 2022 Jun 15;82(12_Supplement):2461.
48. Monge M, Colas E, Doll A, Gil-Moreno A, Castellvi J, Diaz B, et al. Proteomic approach to ETV5 during endometrial carcinoma invasion reveals a link to oxidative stress. Carcinogenesis. 2009 Aug;30(8):1288–97. PMID: 19443906
49. Luo X, Li N, Zhao X, Liao C, Ye R, Cheng C, et al. DHRS2 mediates cell growth inhibition induced by Trichothecin in nasopharyngeal carcinoma. J Exp Clin Cancer Res. 2019 Jul 10;38(1):300. PMID: 31291971
50. Pitzer LM, Moroney MR, Nokoff NJ, Sikora MJ. WNT4 Balances Development vs Disease in Gynecologic Tissues and Women's Health. Endocrinology. 2021 May 1;162(7). PMID: 33963381

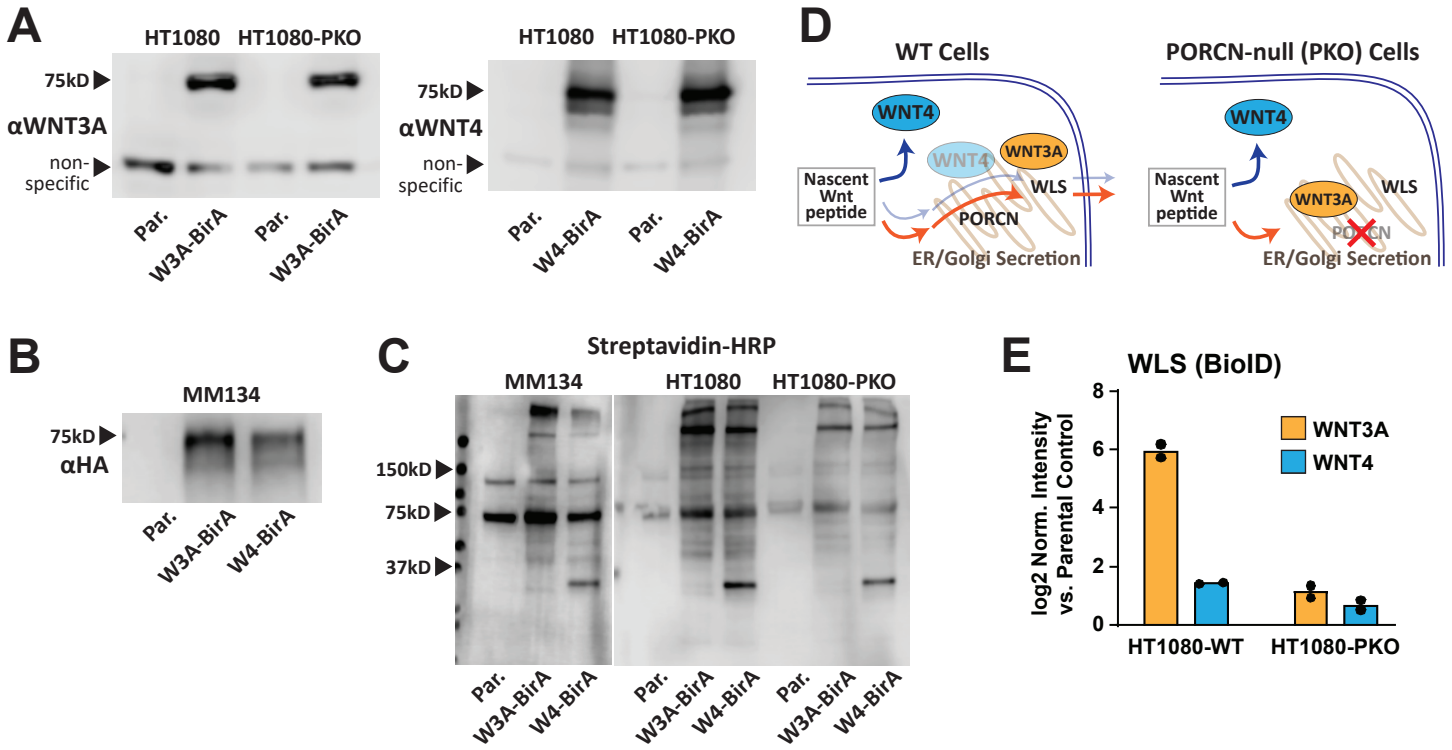

Figure 1. Wnt-BirA proximity biotinylation system differentiates PORCN-mediated Wnt trafficking.
(A-C) Immunoblotting of Parental cell lines (Par.) or cells stably expressing the indicated Wnt-BirA fusion protein. (A) Wnt-BirA fusions are predicted at ~75kD, and are detected by WNT3A or WNT4 antibodies at the expected size. Non-specific band shown as loading confirmation. (B) Wnt-BirA fusions can also be detected at the expected size using an internal HA-tag. (C) Parental and Wnt-BirA expressing cells were treated with 50μM biotin for 24hr, and whole cell lysates were analyzed for the presence of protein biotinylation using streptavidin-HRP conjugate. Wnt-BirA expressing show a broad range of protein biotinylation not observed in parental cells. (D) Model of WNT3A vs WNT4 trafficking in PORCN-wild type vs -knockout contexts. WNT4 trafficking to its intracellular localization is to be PORCN-independent, while WNT3A trafficking to the ER/Golgi and secretion is PORCN-dependent. (E) Mass spectrometry intensity for WLS in the indicated Wnt-BirA model versus parental cell control. Points represent biological duplicate samples.

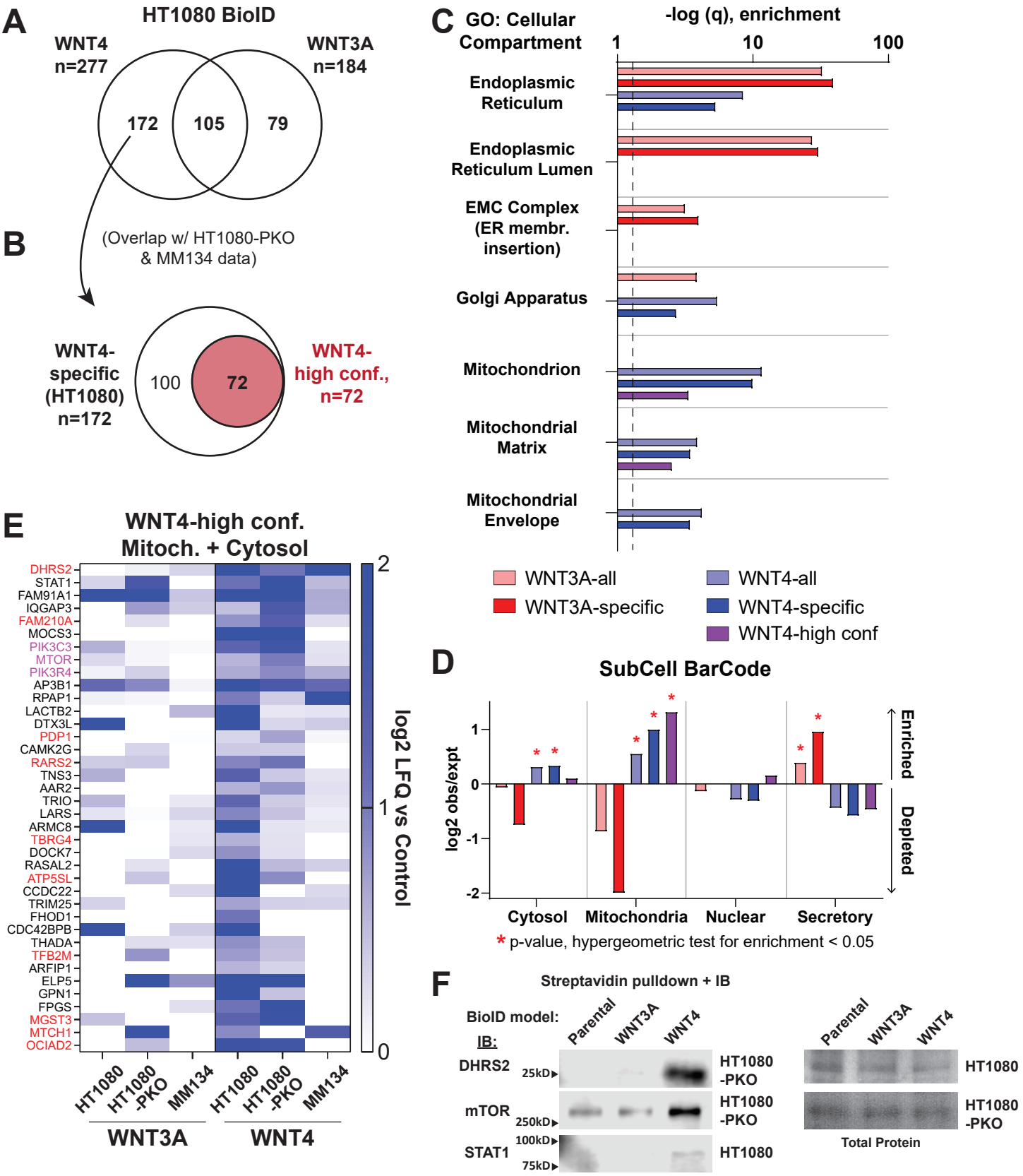

Figure 2. Proximity biotinylation (BioID) supports WNT4 localization to the mitochondria.
(A) Proteins enriched in HT1080 Wnt-BirA versus parental HT1080 cells lacking BirA construct expression. (B) Overlap of proteins identified in HT1080 (panel A) versus HT1080-PKO and MM134 identifies n=72 "high-confidence" WNT4-associated proteins. (C) Gene ontology analysis for cellular compartment for WNT3A- vs WNT4-associated proteins. Dashed line = 1.3 (p = 0.05). (D) Network analysis of WNT3A- vs WNT4-associated proteins via Subcell Barcode. Enrichments against cell line HCC287 background shown; parallel results observed with other cell line background data, e.g. MCF7. (E) Proteins with predicted cytosolic or mitochondrial localization (subcell barcode) among "high-confidence" WNT4-associated proteins. Red = predicted mitochondrial localization, pink = mTOR complex in mitochondrial dynamics, biogenesis, and autophagy. (F) Biotin treatment and streptavidin pulldown was performed as for mass spectrometry studies, and candidate WNT4-associated proteins from (E) detected by immunoblotting. Total protein by Ponceau.

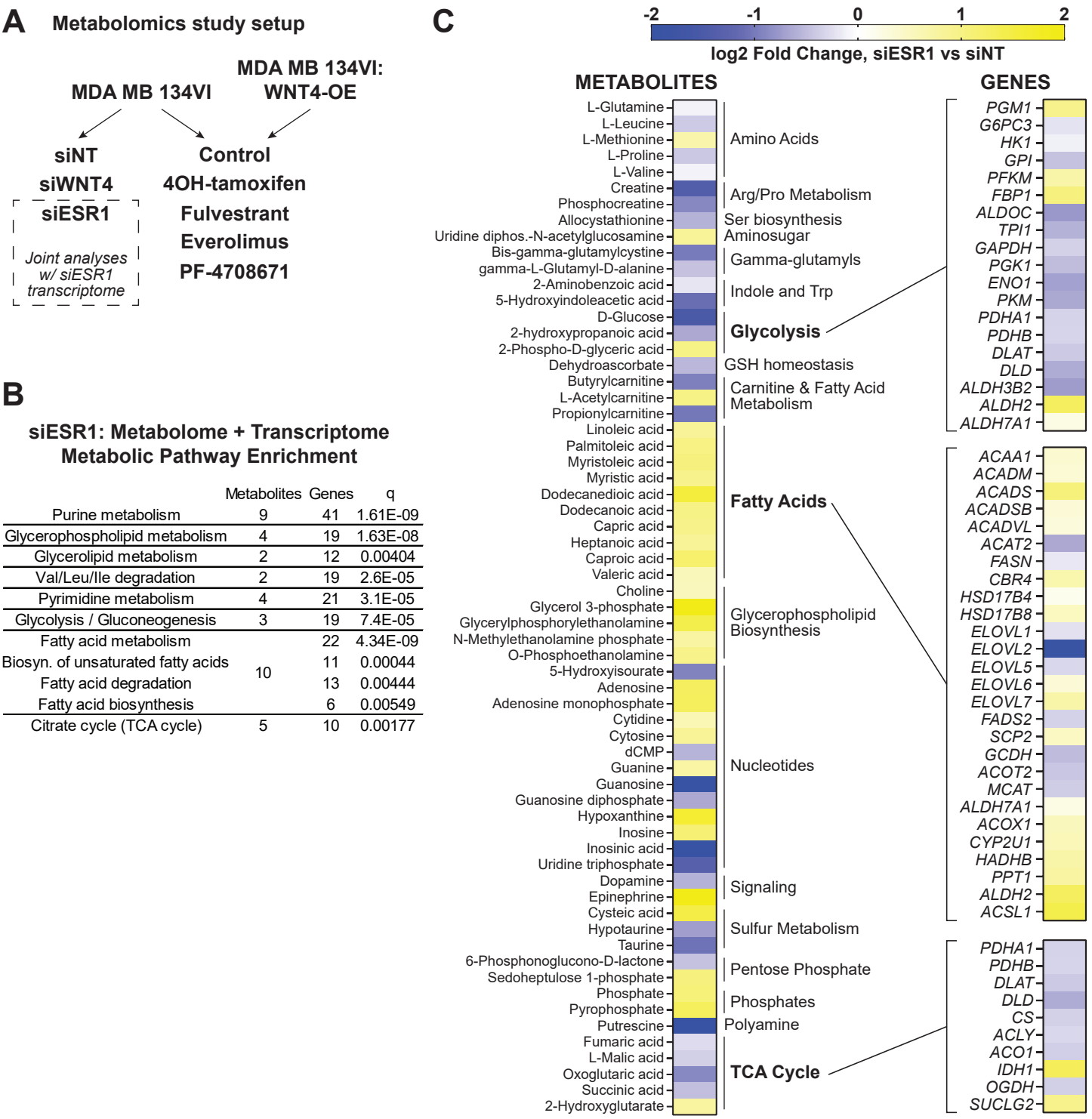

Figure 3. Estrogen receptor regulates glycolysis, oxidative phosphorylation, and fatty acid metabolism in ILC cells. (A) Overall metabolomics study design in MDA MB 134VI ILC cells; all samples in biological triplicate. (B) Joint analysis of trascriptome + metabolome data identifies dysregulated pathways after *ESR1* knockdown. Trascriptome data from GSE171364. (C) Metabolites levels altered by *ESR1* knockdown (left, n=63), with gene expression changes associated with major metabolic mechanisms (right).

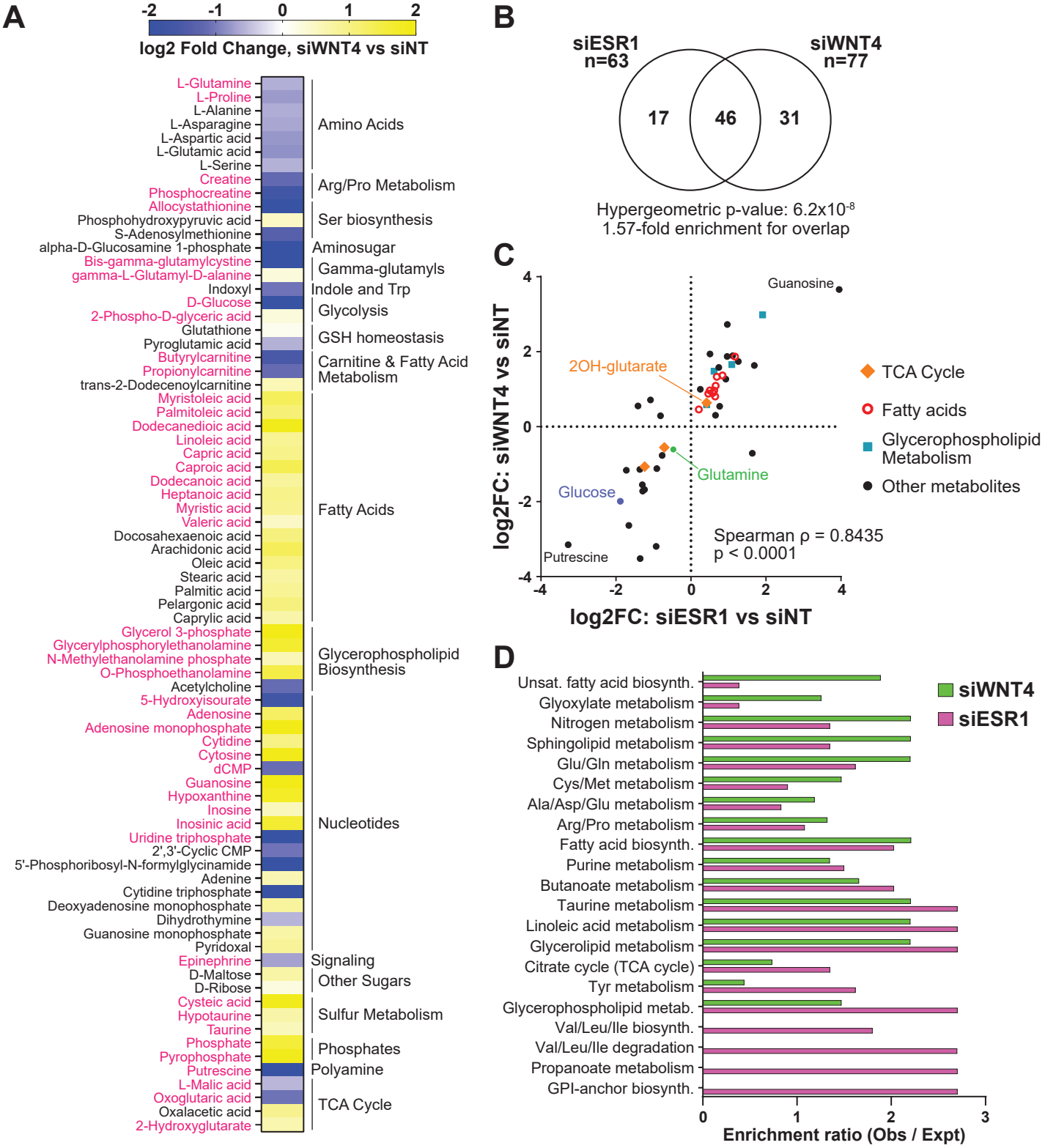

Figure 4. Metabolic effects of WNT4 knockdown closely mirror the effects of ER knockdown.
(A) Metabolite levels altered by *WNT4* knockdown (n=77); pink text indicates a shared affected metabolite with *ESR1* knockdown. (B) Metabolites dysregulated by *WNT4* v *ESR1* knockdown are strongly enriched for overlap. (C) *WNT4* v *ESR1* knockdown effects on metabolite levels are strongly directly correlated, suggesting an overall parallel effect on ILC cell metabolism. (D) Pathway analysis with *ESR1* metabolites (Figure 3C) and *WNT4* metabolites (Figure 4A); $p < 0.4$ in *ESR1* and/or *WNT4* dataset shown.

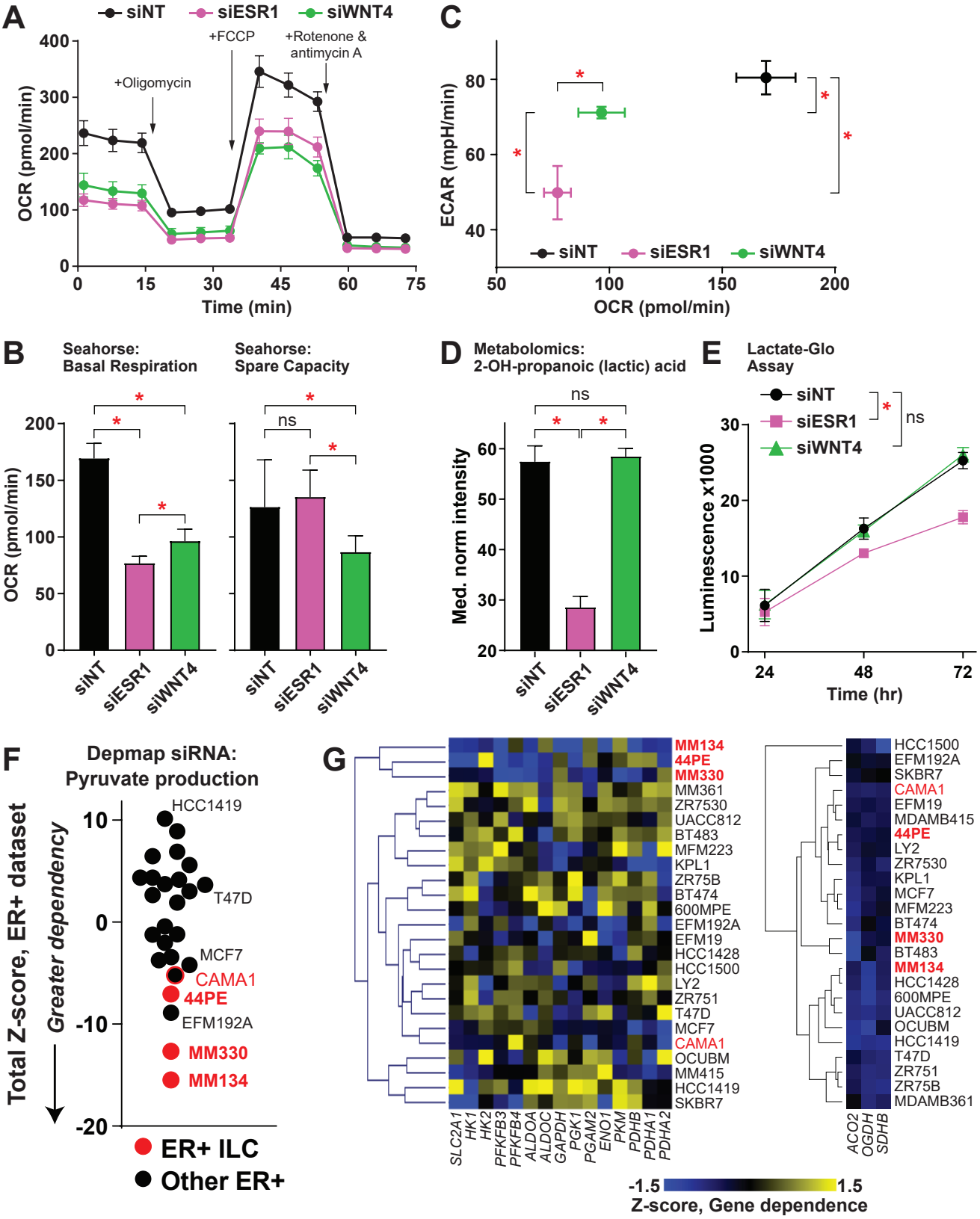

Figure 5. WNT4 knockdown impairs respiration but not glycolysis.
(A) Seahorse MitoStress test in MM134. Points represent mean of 6 biological replicates ± SD. (B) Basal respiration is reduced by ER or WNT4 knockdown, but WNT4 knockdown impairs respiratory capacity. (C) WNT4 knockdown suppresses oxygen consumption (OCR), i.e. respiration (from B), but has a minimal effect on extracellular acidification (ECAR), i.e. glycolysis. (D) From metabolomics data, cellular lactic acid levels are reduced by ER knockdown, but not WNT4 knockdown. (B-D), comparisons by ANOVA with Dunnett's correction. *, adj.p < 0.05. (E) Reduction in lactic acid production was also observed in lactate levels in conditioned medium. *, 2-way ANOVA siRNA effect p<0.05. (F-G) DEMETER2 scores for n=15 genes in pyruvate metabolism were normalized as Z-scores for the subset of ER+ breast cancer cell lines. DEMETER2 siRNA used as ER+ ILC cell line data are not available in Depmap CRISPR-based screens. CAMA1 denoted separately as an "ILC-like" cell line. (F) Total sum of Z-scores for the geneset per cell line. (G) Heirarchal clustering for gene z-scores indicates ER+ ILC lines as an independent cluster. Pyruvate metabolism genes at left, representative TCA genes at right.

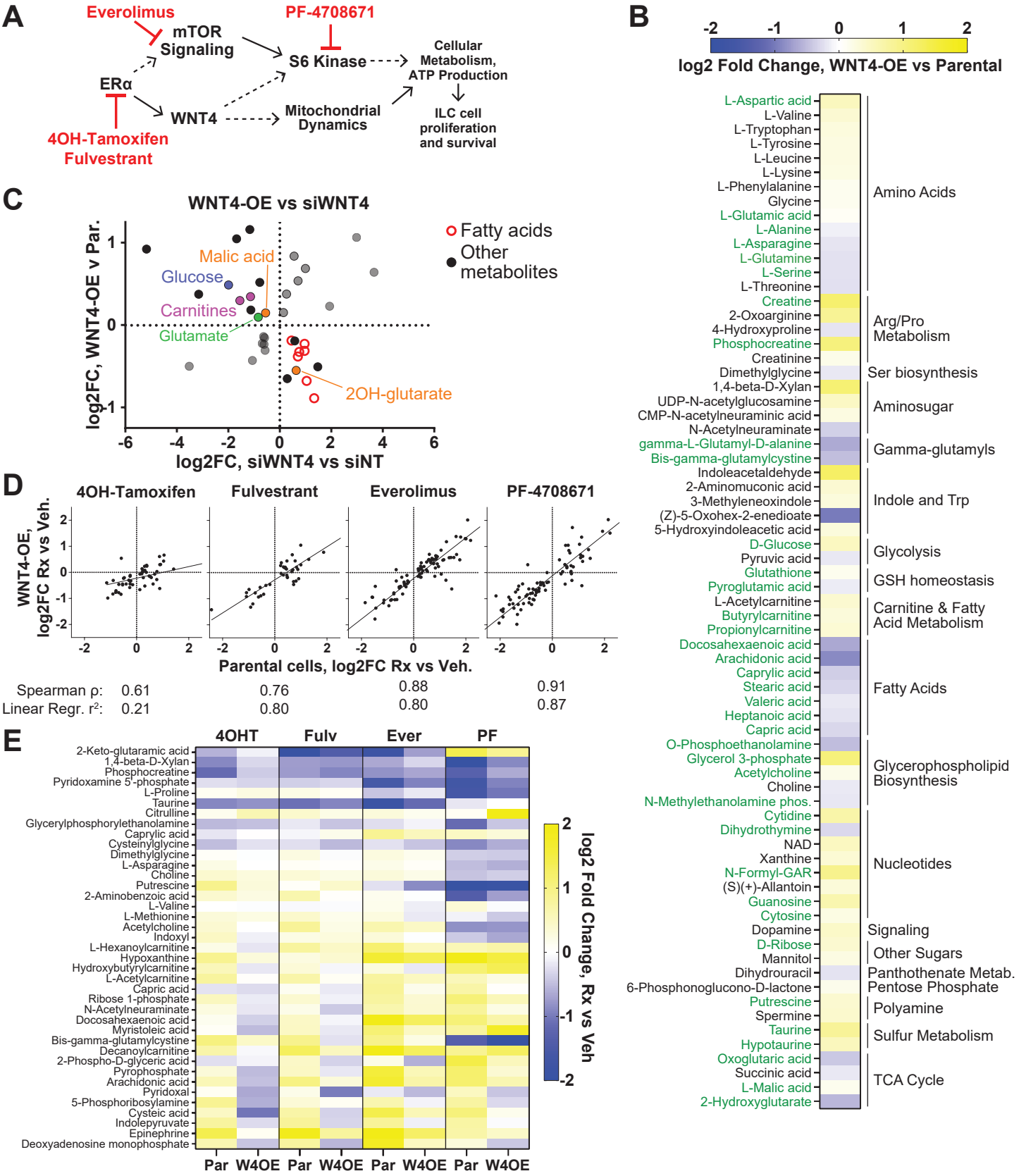

Figure 6. WNT4 over-expression rescues some metabolic effects of ER:WNT4 pathway inhibition.
(A) Small molecule inhibitor targets in current model of ER:WNT4 signaling pathway. (B) Meta-analysis of parental MM134 cells versus WNT4-OE MM134 across drug treatment series (i.e. WNT4 effect controlled for inhibitor effect) identifies n=71 metabolite levels altered by WNT4 over-expression. Green = overlap with siWNT4 dysregulated metabolites. (C) Overall changes in metabolite levels caused by WNT4 knockdown vs WNT4 over-expression are inversely correlated, supporting regulation of associated metabolic pathways by WNT4. (D) Inhibitor effects in parental MM134 vs WNT4-OE MM134 are strongly correlated, but a subset of inhibitor effects are reversed by WNT4 over-expression. (E) Metabolites for which inhibitor effects is decreased by ≥30% for at least 2 inhibitors (n=39).

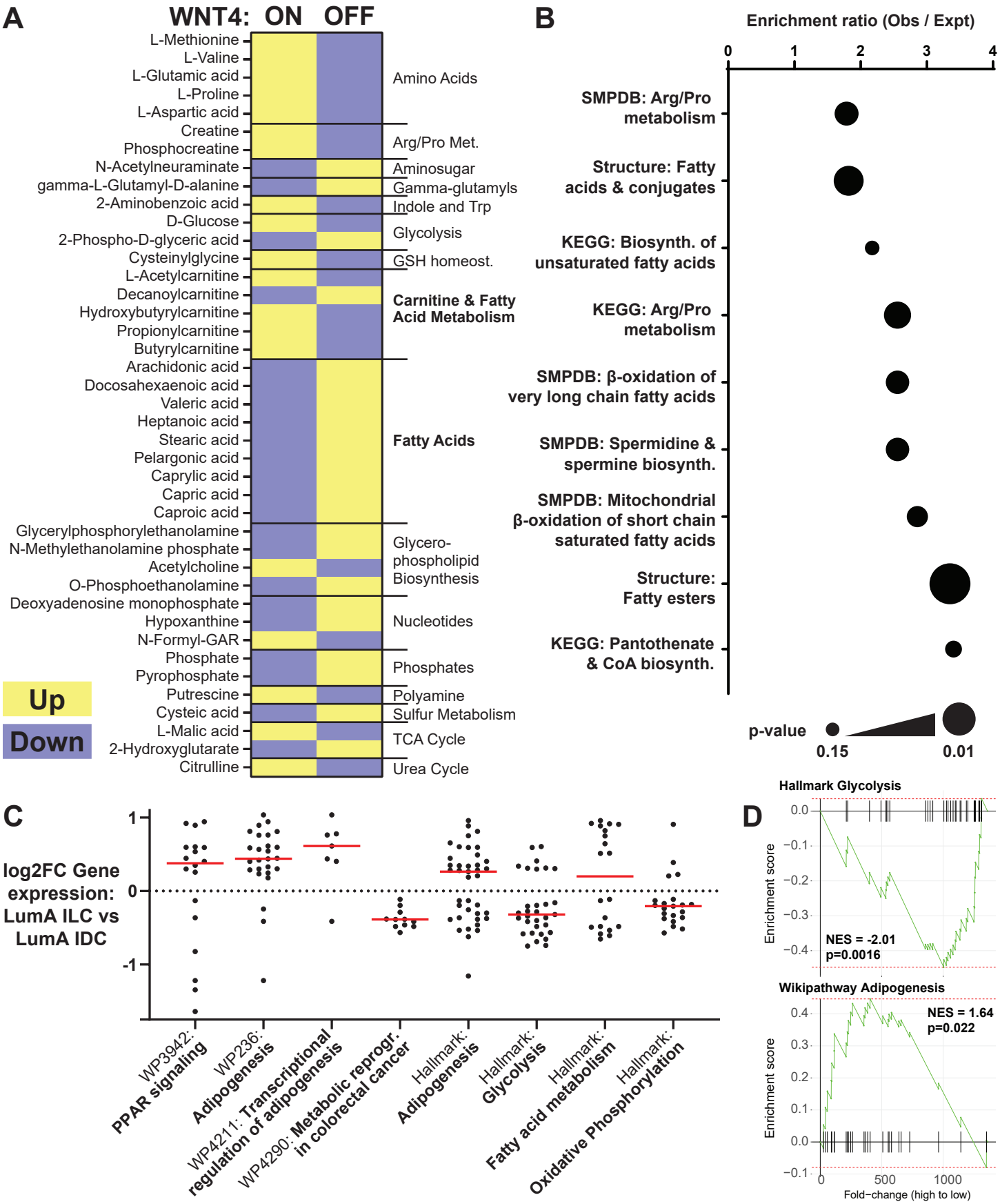

Figure 7. Consensus WNT4-regulated metabolites are enriched for fatty acid metabolism.
(A) Consensus of n=41 metabolites rescued with WNT4-OE and metabolites inversely regulated by WNT4-OE vs WNT4 knockdown. WNT4 ON v OFF corresponds to differential regualtion by WNT4 over-expression vs knockdown, respectively. (B) Pathway analysis of consensus WNT4-regulated metabolites. (C) Gene set enrichment analysis of genes differentially expressed in Luminal A ILC vs Luminal A IDC (n=1360) includes metabolic pathways, with relative gene expression levels in ILC consistent with increased lipid metabolism and decreased glycolysis and OXPHOS. Points = individudal genes (fold-changes from TCGA, Ref X); red bar = median fold change. (D) fGSEA of representative pathways in (C). NES = normalized enrichment score.